

# Metal Hydride-Based Hydrogen Compressor for Hydrogen Microgrid

Shanta Kumar\*, Vinod Kumar, Ajay Kuntal, Yashwant Kumar Saini,

Prabhat Ranjan, Manish Sonker

Hydrogen, Biomass & Waste to Energy Group, NTPC Energy Technology Research Alliance, NTPC Ltd., Greater Noida, Uttar Pradesh, India.

\*shantakumar@ntpc.co.in

**Abstract.** Developing a static metal hydride-based hydrogen compression system with minimal thermal energy requirements and low maintenance is key to building a robust and efficient hydrogen microgrid, where compression plays a critical role. A hydrogen microgrid constitutes a viable approach for the sustainable supply and storage of energy across industrial, institutional, and remote community sectors. The green hydrogen microgrid encompasses renewable energy sources (RES) for electricity generation, in conjunction with integrated systems for hydrogen production, compression, storage, and fuel cell-based energy conversion. To address the challenge of hydrogen compression for high-pressure storage in hydrogen microgrids, a three-stage metal hydride hydrogen compressor (MHHC) was developed. This system overcomes the typical delivery pressure limitation (<100 bar) by compressing hydrogen to pressures exceeding 150 bar. The three-stage MHHC was successfully commissioned and tested, achieving a delivery pressure of 160 bar with heat transfer fluid (HTF) circulated at approximately 45 °C. This approach demonstrates techno-commercial viability, particularly when the MHHC is operated utilizing waste heat or renewable thermal energy sources. Overall, the findings underscore thermochemical hydrogen compression as a robust and energy-efficient approach for hydrogen microgrid applications, effectively meeting the escalating energy demands in remote and hardto-access regions.

**Keywords:** Hydrogen Microgrid, Metal Hydride, Hydrogen compressor

#### 1 Introduction

Hydrogen microgrids provide a reliable and sustainable solution for energy supply and storage in industrial, institutional, and remote settings. Designed for stand-alone operation, these systems support the advancement of the hydrogen economy. Solar-powered hydrogen microgrids offer a practical approach for rural electrification and improve system resilience against outages caused by extreme weather events [1]. The global focus on mitigating climate change has prioritized carbon emission reduction in energy policy, accelerating the transition toward hydrogen-based infrastructure [2]. At the

same time, there is a growing need for eco-friendly ways to produce hydrogen and create green hydrogen supply chains to help reduce carbon emissions from energy systems that rely on fossil fuels.

A microgrid is a localized energy system that integrates distributed energy resources (DERs), such as photovoltaic (PV) panels, waste-to-energy units, and other generators with energy storage systems (e.g., batteries and hydrogen storage) and connected electrical or thermal loads. Equipped with intelligent control systems, a microgrid can operate either in parallel with the main utility grid or independently in island mode [3]. Microgrids are typically classified according to various criteria, including operational mode (grid-connected or stand-alone), supervisory control architecture (centralized or decentralized), electrical configuration (single-phase or three-phase), power type (AC or DC), and the nature of integrated components such as power generation sources, storage systems, and demand-side loads [3].

In a hydrogen-based microgrid, hydrogen is typically produced through water electrolysis powered by renewable energy sources (RES), such as solar energy. At present, green hydrogen production technologies typically operate at pressures of approximately 30 bar [2]. The produced hydrogen is then compressed and stored at high pressure for later use. To meet the water requirements for electrolysis, treated wastewater may be utilized through technologies such as electrodialysis reversal (EDR). For electricity generation, the stored hydrogen is supplied to a fuel cell, which converts it into electrical energy, enabling a clean and reliable power supply.

Because of the low volumetric energy density of hydrogen, it is required to store hydrogen at significantly elevated pressures to ensure its practical applications [4]. This requirement has underscored the importance of developing efficient hydrogen compression systems that are cost-effective, demand low operational energy, and require minimal maintenance to ensure sustainable performance. Conventional mechanical compressors, though widely used, are bulky. Moreover, they generate substantial noise due to moving components and consume considerable electrical energy. Overall, they are facing operational inefficiencies [5].

In contrast, MHHCs offer a promising alternative, utilising thermal energy for hydrogen absorption and desorption. These systems operate silently, as they do not have moving parts. They also require comparatively lower energy input, and hence they are more efficient [5]. Besides having application in hydrogen compression, metal hydrides find extensive utility in hydrogen storage, transportation, purification, and thermal energy storage owing to their unique chemical and thermodynamic properties [5, 6-9]. Notably, MHHCs are capable of supplying hydrogen gas to refueling stations and other storage facilities [10].

It has been projected that the adoption of MHHCs could reduce compression costs by approximately 15-20% relative to conventional methods. Metal hydride-based hydrogen compressors are thermally driven systems capable of compressing hydrogen to higher pressures in either single or multiple stages [11-13].

The working principle of MHHC involves a reversible reaction where a metal (M) with desired characteristics reacts exothermally with hydrogens, producing MH compounds (absorption) and releasing heat (Q) [14]. The reverse reaction, that is, endothermic desorption, occurs at high temperature, whereas compressed hydrogen releases

from the MH bed [13]. The reversible absorption/desorption reactions are represented as shown in Eq. 1, whereas equilibrium of the reaction depends on hydrogen pressure (p), hydrogen concentration in the MH bed (C), and MH bed temperature (T) [14].

$$M(s) + \frac{x}{2}H_2 \rightleftharpoons MH_x(s) + Q \tag{1}$$

Pressurized hydrogen finds various applications in coal-based thermal power plants. At NTPC Energy Technology and Research Alliance (NETRA), demonstration facilities for a hydrogen microgrid powered by solar energy have been established, comprising hydrogen production, compression, storage, and fuel cell-based energy conversion. The compressed hydrogen storage system stores hydrogen up to 200 bar. Currently, mechanical compressors are deployed, resulting in complex, multistage compression systems with high operational and maintenance costs due to their reliance on moving components.

As per the collaborative project on MHHC, an alternate compression system, it has been envisaged to fabricate hydrogen storage reactors of 10000 L of hydrogen storage capacity with hydrogen compression up to 300 bar operating at a temperature (between 80 °C and 300 °C) and a hydrogen supply pressure (between 5 bar and 25 bar).

Metal hydride alloys La<sub>0.8</sub>Ce<sub>0.2</sub>Ni<sub>5</sub>, La<sub>0.5</sub>Ce<sub>0.5</sub>Ni<sub>4</sub>Fe, and Ti<sub>0.8</sub>Zr<sub>0.2</sub>CrMn<sub>0.3</sub>Fe<sub>0.6</sub>Ni<sub>0.1</sub> were utilized in the first, second, and third stage reactors, respectively. Following fabrication, each reactor was individually activated. Subsequently, the stages were coupled to form a complete three-stage metal hydride-based hydrogen compressor (MHHC), which was experimentally demonstrated to compress hydrogen to pressures exceeding 150 bar. The detailed design, development, construction, and performance evaluation of the MHHC system are presented in the authors' previous publication [4]. The present study highlights the continuous hydrogen filling into a high-pressure storage cylinder and its integration with a hydrogen microgrid, specifically targeting industrial application scenarios.

For future deployment in hydrogen refueling stations, particularly in the transport sector, where hydrogen needs to be compressed to 700–800 bar, further design and development may be undertaken, whereas the number of compression stages may be increased, thermal design may be improved, and advanced hydride-forming alloys with higher plateau pressures and faster kinetics may be selected. Plateau pressure is the pressure of the plateau region of PCT isotherm plots representing the relationship between pressure, concentration, and temperature for a metal hydride material, where hydrogen concentration changes while pressure remains almost constant.

The demand for hydrogen will increase manifold with the scaling of carbon capture and utilization (CCU) projects in thermal power plants. Carbon dioxide, captured from flue gas, will be utilized to produce methanol, ethanol, urea, sustainable aviation fuel, etc., using hydrogen to achieve the goals of energy transition. Presently, NTPC has designed an innovative green hydrogen-based microgrid system to supply 200 kW of power round-the-clock, replacing the existing diesel gensets at off-grid Army locations where temperatures drop to -30 °C at an altitude of 4,400 metres, reducing carbon emissions by 1500 tonnes annually [15]. Low-cost options for the hydrogen compressors with fewer maintenance requirements will facilitate achieving the goal of the storage

of hydrogen at high pressure. Under this scenario, the MHHC technology holds strong potential as a scalable, safe, and energy-efficient solution for high-pressure hydrogen delivery in the green hydrogen economy.

# 2 Materials and Methods

The hydrogen microgrid demonstration setup comprises six main components as shown in Fig. 1: (i) a solar photovoltaic power supply system, (ii) a wastewater treatment unit, (iii) hydrogen generation systems, (iv) compressed hydrogen storage systems, (v) a fuel cell-based power generation unit, and (vi) a power delivery system. The schematic consisting of the above systems is shown in Fig. 2.

# 2.1 Solar Photovoltaic (PV) Power Supply System

The electrical energy required for both the electrolysis of water for green hydrogen production and the operation of the electrodialysis reversal (EDR) system for wastewater treatment is supplied by a solar photovoltaic plant with an installed capacity of 4 MWp. The details of the solar plant capacity are mentioned in Table 1.

#### 2.2 Wastewater Treatment Unit.

To address the requirement of the pure water for the electrolysis process (about 12 kg of water for 1 kg of hydrogen generation) under a water-stressed ecosystem, water reuse, the electrodialysis reversal (EDR) process is employed to treat wastewater for electrolysis. In the hydrogen microgrid setup, wastewater is sourced from the Sewage Treatment Plant (STP) operated by the local municipal corporation, and it is treated on-site using the EDR system. Schematic of EDR system is shown in Fig. 3.

The electrodialysis reversal (EDR) system is a membrane-based separation technology that utilizes alternating anion exchange membranes (AEMs) and cation exchange membranes (CEMs) [16, 17]. AEMs contain positively charged groups that allow anion passage while blocking cations; CEMs have negatively charged groups that allow cations and restrict anions [18]. These membranes create concentrated, diluted, and electrode wash compartments.

When an electric field is applied, anions migrate toward the anode and cations toward the cathode. The electrodes, made of titanium coated with mixed metal oxides (Pt, Ru, Rh), facilitate ion transport [19]. To prevent membrane fouling from charged particulates, the polarity of the voltage is reversed every 30–60 minutes, a process known as electrodialysis reversal (EDR), which effectively cleans the membranes by reversing ion flow.

At 75% water recovery and 25 °C, EDR energy consumption ranges from 0.49 kWh/m³ (for 1000 mg/L TDS) to 1.75 kWh/m³ (for 5000 mg/L TDS). The EDR system at NETRA can purify up to one tonne of sewage treatment plant (STP) water per day for use in hydrogen electrolysis. The details of the EDR system are provided in Table 2.

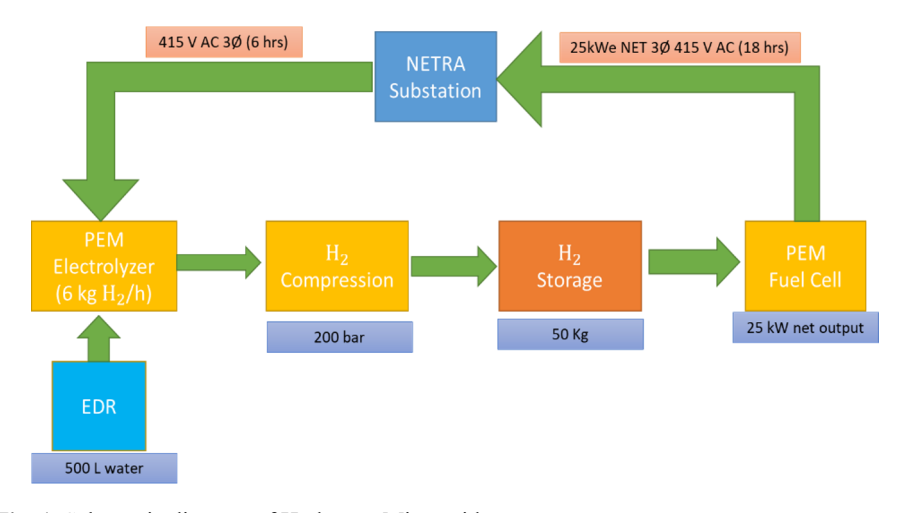


Fig. 1. Schematic diagram of Hydrogen Microgrid.

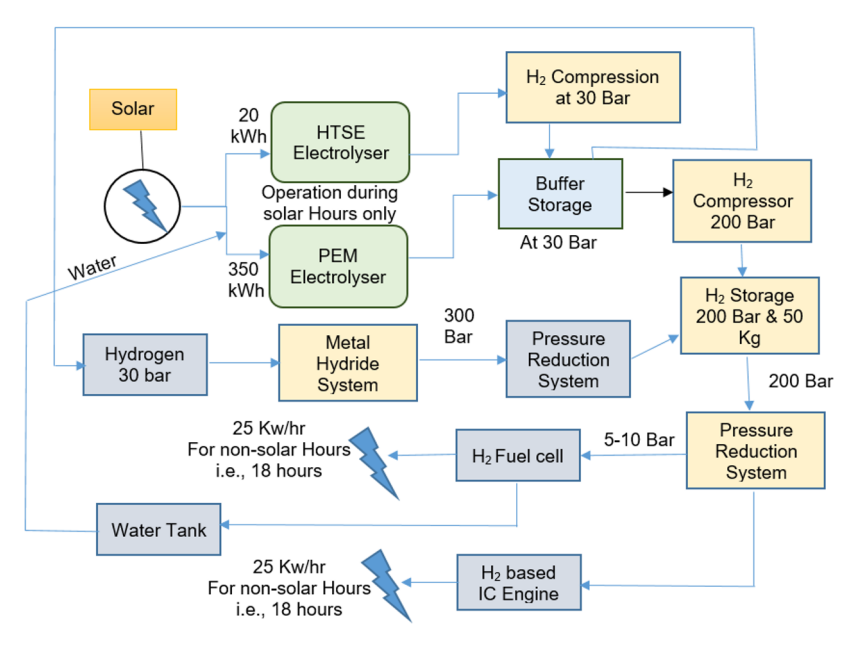


Fig. 2. Constituents of Green Hydrogen Grid (net 25 kWh 24x7).

Table 1. Details of Solar Plant at NETRA

Item	Capacity
Solar Module Rating (Wp)	545
Inverter Rating (kW)	3300
Total Modules in Plant	7410
Plant DC Capacity (kWp)	4038

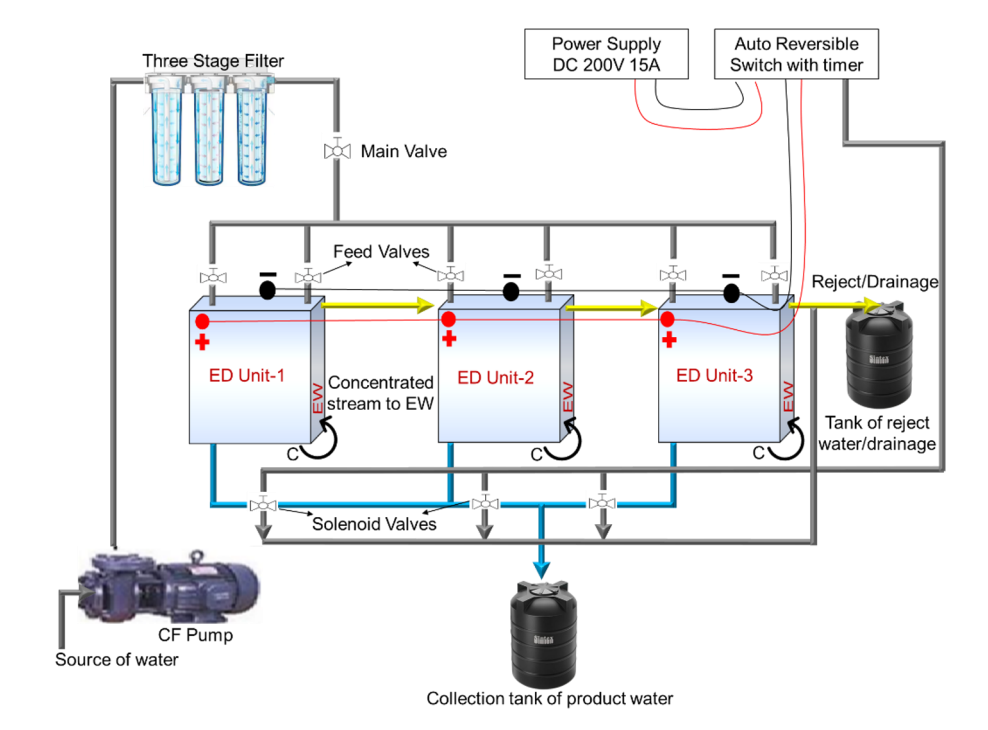


Fig. 3. Schematic drawing of EDR system

Table 2. Details of the EDR system at NETRA

Parameters	Value	
Capacity of the plant	1000-1100 L/h	
TDS of Feed water	1500-2500 mg/L	
Size of the unit/no. of unit	80 cm * 40 cm / 3	
Number of cell pair of membranes in each unit	120	
Running time	8h then 15 minutes reversal	
EDR Inlet/Outlet (using APHA test	pH: 8.6 / 7.7	
method)	Conductivity (µs/cm): 1760 / 905.7	
	TDS (ppm): 1056/541.4	
	Turbidity (NTU): 0.48/0.38	
	Chloride [Cl <sup>-</sup> ] (ppm): 259.5/100.7	
	Ca Hardness (ppm): 130/40	
	Mg Hardness (ppm): 122/50	
	Total Hardness (ppm): 252	
	P-Alkalinity (ppm): 28/-	
	M-Alkalinity (ppm): 404/246	

# 2.3 Green Hydrogen Generation

A polymer electrolyte membrane (PEM)-based electrolyser system has been installed at NETRA to produce 6 kg/h of hydrogen with the designed power input of approximately 350 kW. Alternately, a solid oxide electrolytic cell (SOEC) has also been installed to electrolyse high-temperature steam with temperatures around 800–850 °C, producing approximately 0.5 kg/h of hydrogen. Notably, the high-temperature steam electrolyser (HTSE) consumes around 20% less electricity compared to the PEM-based system, owing to improved thermodynamic efficiency at elevated temperatures.

**PEM-based electrolyser**. In a PEM electrolyzer, when water is introduced at the anode and a direct current (DC) is applied across the electrodes, the platinum-coated anode catalyzes the electrolysis reaction, splitting water into oxygen gas, protons (H<sup>+</sup>), and electrons. The DC potential drives the electrons through an external circuit toward the cathode, while the polymer electrolyte membrane selectively conducts the protons from the anode to the cathode. At the cathode, these protons combine with the incoming electrons to form hydrogen gas (H<sub>2</sub>). The membrane permits only the transport of positive ions, thereby ensuring the spatial separation of hydrogen and oxygen gases, which can then be collected and stored independently. The membrane, serving as the electrolyte, is typically made of perfluorosulfonic acid (PFSA) or perfluorocarboxylic acid (PFCA) polymers, valued for their high proton conductivity and stability [20]. The schematic of PEM electrolyser has been shown in Fig. 4 and details are listed in Table 3. The power requirement is sourced from solar plant as shown in Fig. 5.

Anode 
$$2H_2O \rightarrow O_2 + 4H^+ + 4e^-$$
 (2)

Cathode 
$$4H^+ + 4e^- \rightarrow 2H_2$$
 (3)

HTSE based electrolyser. As shown in Fig. 6, the Solid Oxide Electrolytic Cell (SOEC)-based High-Temperature Steam Electrolyser (HTSE) enables the electrolysis of steam at elevated temperatures (~850 °C), offering significantly higher efficiencies compared to conventional alkaline or polymer electrolyte membrane (PEM) electrolysers. HTSE cells are composed of oxygen ion-conducting ceramic membrane electrolytes. A dense ceramic electrolyte is sandwiched between two porous, electronically conductive electrodes that possess high catalytic activity. In this system, ultrapure steam is preheated to the required operating temperature and introduced into the cathode side of the HTSE unit, where reactions occur (Eq. 4) [21].

Cathode Reaction 
$$2H_2O + 4e^- \rightarrow H_2 + 40^{2-}$$
 (4)

The resulting oxygen ions (O<sup>2-</sup>) migrate through the solid electrolyte under the influence of the electric field and are oxidized at the anode, releasing oxygen gas via the reaction (Eq. 5) [22]:

Anode 
$$0^{2-} \to \frac{1}{2} O_2 + 2e^-$$
 (5)

The main subsystem of the SOE system has been enlisted in Table 4.

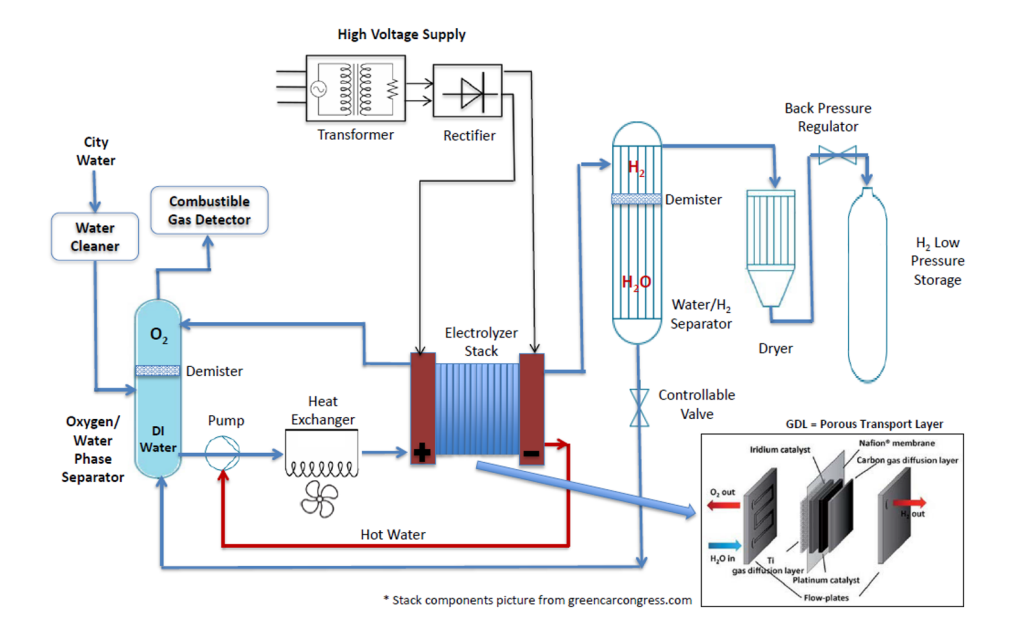


Fig. 4. Schematic of Polymer electrolyte membrane (PEM) electrolysis

Table 3. Detail of PEM Electrolyser

Item	Description
Model of Electrolyser	Mark 1
Technology	PEM
Hydrogen Production Rate	6 kg/h
Stack operating temperature	Max. of 85 degree C
Power rating (DC)	300 kW
Inlet Water (Normal)	2.7 L/min
Inlet water pressure	30 psi (2.1 bar)
Rejected water	1.3 L/min
Material of construction (H2 pressure reduc-	Valve body: SS304, Internal: SS316, piping
tion system)	& fitting SS304 % SS316
AC Power consumption	5.5 kWh/Nm3 H2 or 55 kWh/kg H2
Start-up time (from off state)	10 min
Ramp-up time (minimum to full load)	5 s
DI water consumption	1.4 L/min (quality of water with less than 2 micro-siemens/cm)
Coolant	Liquid cooled (glycol-water mixture)
Interface connection	H2 product port75 in
	O2 and H2 vent port – diluted in plenum.
	Inlet water line diameter- 1 in
	Drain port (rejected water)5 in
Cost	Rs. 1.31 Cr



Fig. 5. Site photograph of the hydrogen microgrid.



Fig. 6. Site photograph of the TSE System showing various components.

Table 4. Main Sub-system of SOE system

Physical Devices	Control Devices	System Wide Setting	
Solid Oxide electrolysis cell (SOEC)	Classical feedback	System components	
stacks and Hotbox assembly	Controllers		
Heat exchangers (HXs),	Feedforward controllers		
Molten salt bath,	Temperature control		
	valves (TCVs)		
H2-O2 steam generator (combustor)	Control bus		
Electric Topping Heaters (ETHs)	Other Equipment		
Hydrogen/Steam Mixer	H2 Leak Detector	-	
Hydrogen recycle loop	Gas Purity Analyzer		
Flash drum	HVAC		
Switchyard	Chiller Unit		
Mass flow controllers			
Electrical Panel			

# 2.4 Power Production System

The compressed hydrogen is used for electricity generation through either a fuel cell system with a 25-kW capacity or a hydrogen-fuelled internal combustion engine. According to the design of the hydrogen microgrid at NETRA, approximately 2 kg of the stored hydrogen per hour is fed into the fuel cell to generate electricity, supplying 25 kWe into the microgrid during non-solar hours (18 hours). The details of the fuel cell have been listed in Table 5. The typical fuel cell at NETRA is shown in Fig. 7.

Polymer Electrolyte Membrane (PEM) fuel cells are high-efficiency (50–60%) electrochemical systems that convert hydrogen into electricity and heat. They consist of platinum-catalyzed anode and cathode electrodes separated by a proton-conducting, water-based acidic polymer membrane [22]. At the anode, hydrogen is split into protons and electrons; the electrons generate electricity via an external circuit, while the protons travel through the membrane to the cathode, where they react with oxygen to form water and release heat. Bipolar plates provide structural integrity, enable electron conduction, distribute gases, and manage thermal output. A single PEM cell generates 0.5–0.7 V under standard operating conditions.

# 2.5 Compressed Hydrogen Storage Systems

Hydrogen produced from the PEM electrolyser at  $\sim$ 10 bar and from the SOEC system at  $\sim$ 0.5 bar is compressed to  $\sim$ 30 bar using diaphragm compressors and fed into a common buffer tank. Then, hydrogen is further compressed up to  $\sim$ 200 bar using a two-stage diaphragm compressor as shown in Fig. 8 and stored in a high-pressure storage system. The details of the diaphragm compressor are listed in Table 6. As shown in Fig. 9, the storage unit consists of 20 cylinders arranged in five stacked layers on a steel frame, enclosed with safety provisions in compliance with PESO regulations.

Table 5. Details of fuel cell.

Technical Data	Description
Main system parameters	The system is based on the FC stack platform. Output power is 40 kW, maximum current is 334 A, system output voltage is 125-250 V, load modulation is 30-100 %, and operation modes are idle, stand-by, run mode, and emergency
Anode (Hydro- gen) Line Cathode (air) Line	Swagelok standard fittings, hydrogen pressure required is between 8 and 12 barg, hydrogen quality should be as per ISO 14687 It includes an integrated compressor and 3-phase inverter, fresh air supply for the cathode sub-system, depleted air extraction, and drainage of condensed water.
Cooling Line	Liquid cooled, Tin- 65-70 OC, Tout-75-80 OC, coolant is a mixture of De-ionized water and Glycol, liquid to air heat exchanger, connection ports/tubes
Communication Means	Based on the CAN interface (CAN 2.0B Extended frame)
Dimension of Metal enclosure (L X W X H)	920 X 920 X 920 mm



Fig. 7. Photograph of the Fuel Cell.



Fig. 8. Site photograph of the Diaphragm Compressor



Fig. 9. Site photograph of the Hydrogen Storage.

Table 6. Details of the Diaphragm Compressor

Parameter	Value		
Compressor Model/Type	D1-70/100, Metal diaphragm type, electrically driven, water cooled, two stages		
Suction Pressure (Temperature)	27 barg (Ambient)		
Maximum discharge pressure	200 barg,		
Operating media/Flow rate	Hydrogen gas, 85 SCMH		
H2 purity at compressor inlet/outlet	99.99%/99.99%		
Construction Material	Process Head: 300 series stainless steel.		
	Check Valves: 316 SS, 17-4 PH, Vespel peak, Process seal-Viton, Oil Seal – Buna, Diaphragm		
	(Gas/Middle/Oil) -301 SS, Leak detection -316		
	SS, Brass		
Cost	Rs. 1.75 Cr.		

#### **2.6 MHHC**

Metal hydride-based thermochemical hydrogen compression works on the characteristic absorption-desorption cycle at different sets of temperature and pressure conditions. The process of development of multi-stage MHHC has been shown in Fig. 10.

**Design and Development of MHHC.** The 3-stage MHHC has been designed and developed to meet the estimates of parameters listed in Table 7. Design consideration for the MH reactors are taken to optimize the hydrogen compression capacity, compression ratio, thermal efficiency, and mass of the reactors, while maximizing mechanical and



Fig. 10. Process of development of multi-stage MHHC

structural strength to withstand high pressures within the MH bed [23, 24, 25]. The design guidelines in Division 2 of Section VIII of the American Society of Mechanical Engineers (ASME) Boiler and Pressure Vessel Code were followed [26, 27]. Based on the above design considerations, 19 tubes were used in each reactor of the MHHC. The outer diameter of 33.4 mm, with a wall thickness of 4.55 mm for all the reactors. The length of all 19 tubes for Stage 1 and Stage 2 is 1000 mm. For the Stage 3 reactor, all 19 tubes have a length of 1200 mm. Tubes are arranged on concentric circles: one tube is kept in the centre, 6 tubes are arranged in the middle circle with a radius of 43.44 mm, and 12 tubes are arranged in the outer circle with a radius of 86.8 mm, equally distributed. The tube sheet has a diameter of 232.5 mm and a thickness of 14.8 mm.

To prevent the escape of metal hydride powder along with hydrogen during desorption, one end of each tube was capped by welding tubular sintered porous filters. The pore size of the filters was 0.5  $\mu$ m, and the external diameter was 13 mm. SS316 material was used for manufacturing these filters. Another end had provision for using thermocouples as well as alloy filling into the reactors. The details of the developed 3-stage metal hydride-based compressor have been delineated in Table 8.

The absorption time and the reacted fraction are two important parameters for hydrogen filling of a cylinder using the MHHC. Absorption time is the duration of hydrogen absorption indicated by the rise in temperature until the temperature reaches the initial HTF temperature and reacted fraction is the ratio of the amount of hydrogen absorbed  $(m_{abs,H_2})$  in the MH bed to the maximum storage capacity of the alloy in the MH bed.

Parameters	Value (available)
Maximum source temperature	120-130°C
Available hydrogen pressure at source (PEM based electrolyzer at NETRA generating hydrogen at 10-12 bar)	10-20 bar
Desired delivery pressure (hydrogen is stored at 200 bar at NETRA)	200-300 bar
Storage capacity for compressed hydrogen	6000 L of H <sub>2</sub>
Stages of MHHC	Three stages
Absorption temperature (chosen)	5-20°C
Desorption set point (chosen)	80-90°C

**Table 7.** Design considerations for the selection of metal alloys.

**Table 8**. The details of the developed 3-stage metal hydride-based compressor.

Parameters	Details
Alloy for the first-stage reactor	La <sub>.0.8</sub> Ce <sub>0.2</sub> Ni <sub>5</sub> (AB <sub>5</sub> type), (suitable for supply pressure 3 bar, output pressure 200 bar [28])
Alloy for the second-stage reactor	La <sub>0.5</sub> Ce <sub>0.5</sub> Ni <sub>4</sub> Fe (AB <sub>5</sub> type), can compress hydrogen up to 32 bar at ~60 °C, doped Fe enhances interaction with the hydrogen atom [29]
Alloy for the third-stage reactor	$Ti_{0.8}Zr_{0.2}CrMn_{0.3}Fe_{0.6}Ni_{0.1}$ (AB <sub>2</sub> type)
Benefits of alloying	Regulates the hydrogen plateau pressure and improves the reaction kinetics [30]
Procurement of alloy	5-10 mm alloy granules were procured from a China-based agency, M/s Zhongke Scientific & Technical Co. Ltd.
The quantity of alloys filled in the reactors	25-30 kg of powdered alloys (as 5-10 mm granules using planetary ball mills)
Storage capacity (wt.%), absorption pressures, and desorption pressures of alloys	The storage capacity (wt.%) of La.0.8Ce0.2Ni5, La0.5Ce0.5Ni4Fe, and Ti0.8Zr0.2CrMn0.3Fe0.6Ni0.1 are 1.42, 1.3 and 1.3 respectively, absorption pressures at 5°C are ~3.68, ~11.3, and ~55.3 bars respectively, and desorption pressures at 60°C are ~10.28, ~31.54, and ~145.7 bars respectively.
Densities of chosen MH alloys	The density ( $\rho_{MH}$ ) of AB <sub>5</sub> -type alloys (used in stages 1 and 2) is $\sim$ 8400 kg/m³ (approximated), and that of AB <sub>2</sub> -type alloys is $\sim$ 6000 kg/m³ (approximated).

#### 3 Results and Discussion

The temperature, the hydrogen mass flow rate and the HTF flow rate are the important parameters, which determine the compression and hydrogen filling performance of the MHHC. Temperatures are measured using five thermocouples, placed inside the metal hydride bed longitudinally at distinct locations, and two thermocouples are set to measure the HTF inlet as well as outlet temperatures. Hydrogen mass flow rate in the hydrogen line is measured using a Coriolis flow meter (CFM). HTF flow rate is measured by a positive displacement flow rate meter (type: helix, make: ATN Instruments).

# 3.1 Demonstration of the coupling of reactors for continuous operation of the three-stage MHHC

The 3-stage MHHC are set up at NETRA as shown in Fig. 11. For the continuous operation of the three-stage MHHC, two MH reactors for each stage were arranged in such a way so that while one cylinder is absorbing hydrogen, the other cylinder is taken into service for desorption of hydrogen. Further, tubes, tube fittings, and valves were fitted for the gas circuit. For effective heat transfer during absorption (removal of heat) and desorption (supply of heat), the hot bath and the cold bath were utilised for recirculation of HTF (water) at constant temperature.

Coupling of reactors (Stage I to Stage II). The Stage 1 reactor was sensibly heated to 70 °C, leading to a pressure rise up to 55 bar. At this time, the Stage 2 reactor was cooled and maintained at a temperature of  $\sim 10$  °C. 245 g of hydrogen was transferred from the Stage 1 reactor to the Stage 2 reactor, and consequently the pressure of the Stage 2 reactor bed rose to 25 bar. Temporal variation of bed temperature during hydrogen transfer from the Stage 1 to the Stage 2 reactor has been shown in Fig. 12.

Coupling of reactors (Stage II to Stage III). After absorption of hydrogen, the Stage 2 reactor was heated to raise the temperature up to 90 °C and the pressure also rose up to 100 bar. Then, HTF with the temperature ~5 °C was circulated through the Stage 3 reactor for cooling and maintaining its temperature at ~5 °C. Under this condition 275 g of hydrogen was transferred from Stage 2 to Stage 3. Temporal variation of bed temperature during hydrogen transfer from the Stage 1 to the Stage 3 reactor has been shown in Fig. 13. Then the Stage 3 reactor was sensibly heated to ~95 °C. Variation of hydrogen pressure during sensible heating of stage 3 reactor to cylinder have been shown in Fig. 14.

**Storage of compressed hydrogen**. After hydrogen was absorbed in the Stage 3 reactor bed, it was heated to raise the temperature up to 45 °C, leading to a reactor bed pressure of 160 bar. Compressed hydrogen was then transferred to refill an empty gas cylinder up to 60 bar in one cycle. Variation of hydrogen pressure during sensible heating of the stage 3 reactor has been shown in Fig. 15, and the temporal variation of bed temperature during hydrogen transfer from Stage 3 to the cylinder for storage of compressed hydrogen has been shown in Fig. 15.



Fig. 11. Site photograph of the setup of the 3-stage MHHC.

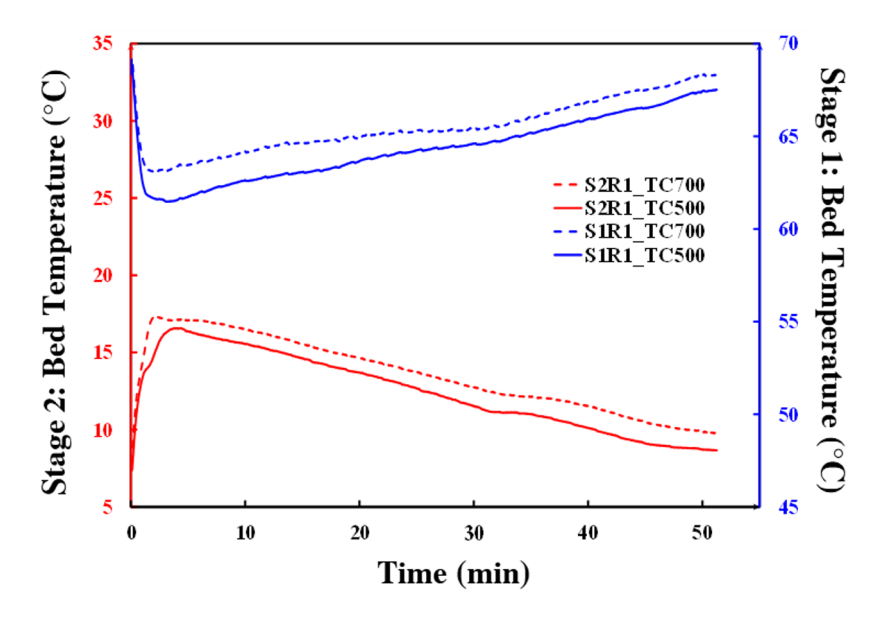


Fig. 12. Temporal variation of bed temperature during hydrogen transfer from stage 1 to stage 2 reactor.

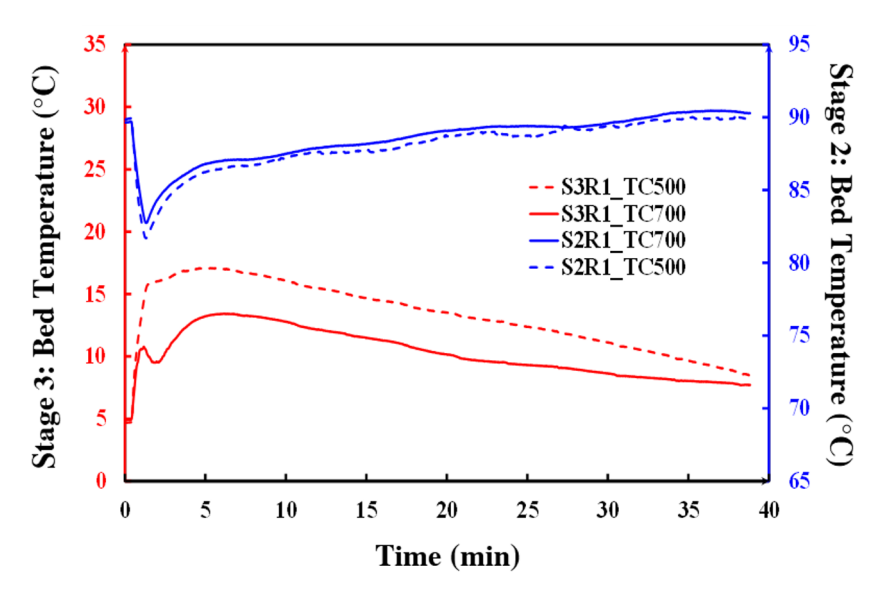


Fig. 13. Temporal variation of bed temperature during hydrogen transfer (coupled stage 2 and stage 3 reactors).

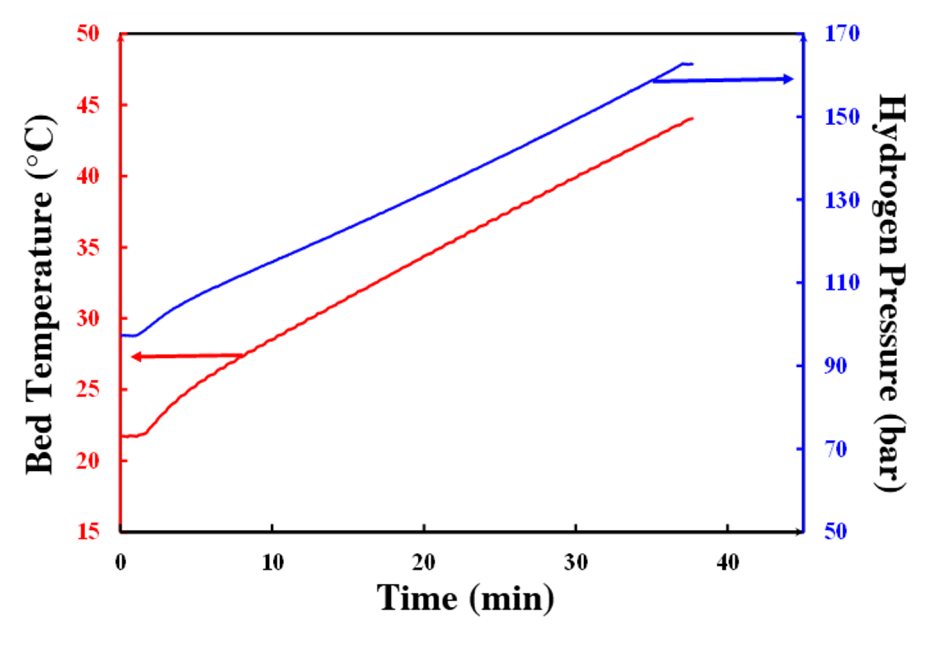
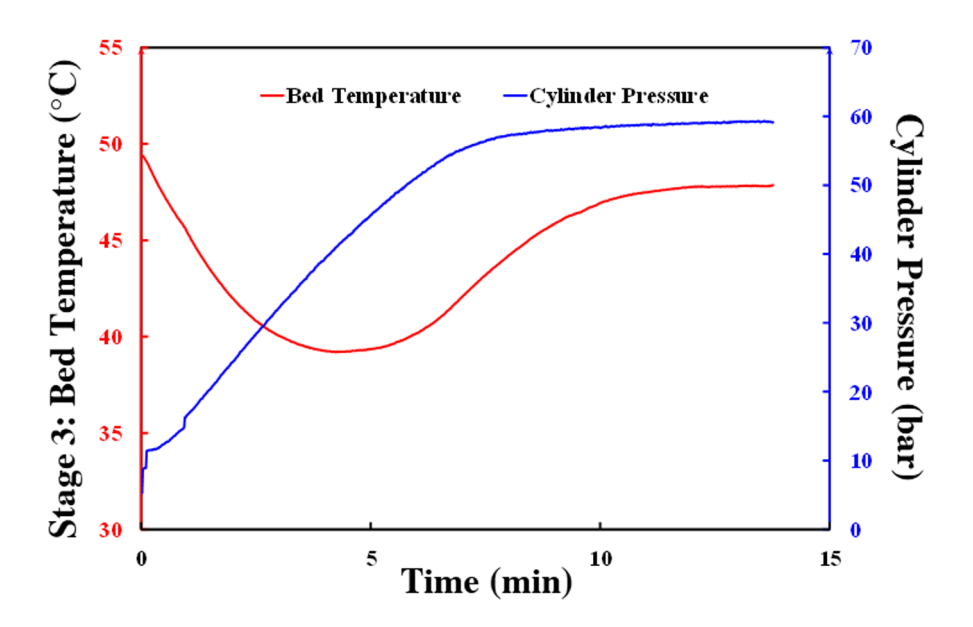


Fig. 14. Variation of hydrogen pressure during sensible heating of stage 3 reactor to cylinder.



**Fig. 15**. Temporal variation of bed temperature during hydrogen transfer from stage 3 reactor to cylinder.

# 3.2 Thermal Performance Analysis

The heat flow schematic for the complete cycle consisting of absorption and desorption has been shown in Fig. 16 for reactor 1.

**Thermal energy consumption.** All three stages' reactors were sensibly cooled alternately after desorption to facilitate absorption efficiently. Heat flow during cooling, exothermic absorption, heating, and endothermic desorption was shown in Fig. 17. As shown in Eq. 6, the cumulative thermal input ( $Q_{total}$ ) required for completion of a single compression cycle, including cooling, heat removal during absorption, and heating for desorption, includes sensible heat (Eq. 7) and reaction heat (Eq. 8), taking their absolute values.

$$Q_{total} = |Qsensible| + |Qreaction|$$
 (6)

$$Q_{Sensible} = |Q1sensible| + |Q3sensible| + |Q5sensible| + |Q7sensible| + |Q9sensible| + |Q11sensible|$$
 (7)

$$Q_{Reaction} = |Q2reaction| + |Q4reaction| + |Q6reaction| + |Q8reaction| + |Q10reaction| + |Q12reaction|$$
 (8)

The mass of each reactor is 61 kg, and the mass of hydride material filling the reactor is taken to be 25 kg (maximum wt.). So, the total mass of each reactor system is 86 kg. The specific heat is approximated for each reactor system as 500 J/(kg.K) [4]. So, the total estimated sensible heat for cooling as well as heating, taking their modulus, is 20.64 MJ using Eq. 9. Here,  $\Delta T_1$ ,  $\Delta T_2$ , and  $\Delta T_3$  represent the temperature differences between the desorption temperature (~90°C) and the optimum absorbing temperatures of ~15°C, ~10°C, and ~5°C for Stage I, Stage II and Stage III reactors, respectively.

$$Q_{sensible} = \sum_{i=0}^{n} (m_i \times c_i) \times \Delta T = 2mc (\Delta T_1 + \Delta T_2 + \Delta T_3)$$
 (9)

Reaction heat is estimated from Eq. 10. Here, the enthalpy of absorption ( $\Delta H_a$ ) and the enthalpy of desorption ( $\Delta H_d$ ) are obtained from P-C-T [4]. Here,  $m_{H2}$  is the mass of hydrogen absorbed/ desorbed, and  $M_{H2}$  is the molar mass of hydrogen.

$$|Qreaction| = m_{H_2} \times \Delta H_a/M_{H_2} + m_{H_2} \times \Delta H_d/M_{H_2}$$
 (10)

By measuring the mass of hydrogen absorbed/desorbed for Stage I, Stage II, and Stage III reactors, 307 g, 388 g, and 275.5 g, respectively, and corresponding enthalpy of formations for absorption/desorption are 27 kJ/kg, 27.5 kJ/kg/23.5 kJ/kg, and 23.8 kJ/kg and 18.3 kJ/kg, respectively, total reaction heat obtained was ~17.2 MJ. For compressing 275.5 g (3.1 Nm³) of hydrogen, the required total thermal energy is about 36.2 MJ or 10.1 kWh, which is higher as compared to power consumed by a diaphragm compressor (i.e., 2.45 kWh/kg H<sub>2</sub>) compressing hydrogen from 30 bar to 200 bar installed at NETRA [4]. Sourcing thermal energy from waste energy or solar energy will enhance the efficiency of the system. Utilizing the phase change material (PCM), the reaction heat released during absorption can be stored and then can be recycled for the hydrogen desorption processes, enhancing thermal efficiency [23].

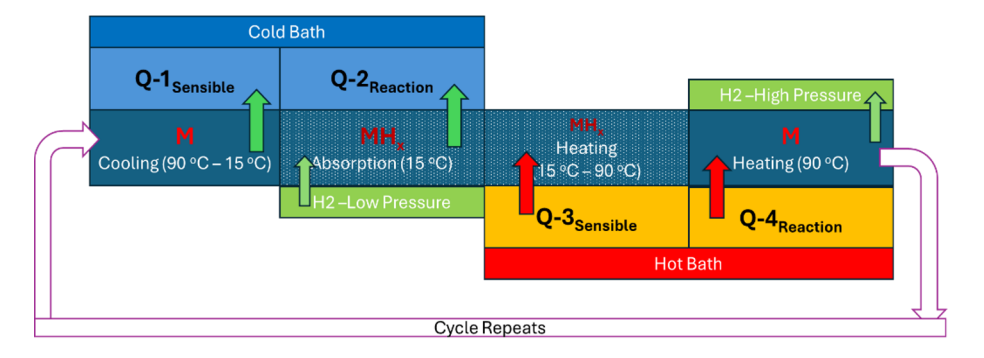


Fig. 16. Heat flow during absorption and desorption phases of reactor 1

# 3.3 Comparative Analysis of MHHC

Though electrochemical hydrogen compressors can perform with high efficiencies, reaching up to 80–95%, they are not taken in applications due to several limitations, such as response towards hydrogen impurities, limited hydrogen throughput, and higher cost implications. Further, mechanical compressors can provide higher efficiency and throughput, but their function is associated with high noise levels, high electrical power, and frequent maintenance work.

In contrast, the developed MHHC in this study exhibited a thermal efficiency of approximately 5%. Despite the lower thermal efficiency, MHHCs offer distinct advantages: they are inherently safer, simpler in design, have lower operational costs, and possess the added benefit of hydrogen purification during the absorption—desorption cycle.

The performance evaluation of the developed three-stage MHHC provides improved hydrogen compression as compared to the similar three-stage designs developed as listed in Table 9 [31, 32].

The hydrogen throughput of about 134 L/min was achieved by discharging over 200 g of hydrogen, filling the empty cylinder in 17 min during the test as described above. Based on this result, taking a total of 75 kg of alloy filling the reactor, the specific productivity of 107.2  $L_{H_2}$  kg<sup>-1</sup>h<sup>-1</sup> was achieved as compared to the productivity of 67.2  $L_{H_2}$  kg<sup>-1</sup>h<sup>-1</sup> achieved by the 6-stage MHHC developed by HYSTORE [33].

MHHC/Yr	Stage I desorp- tion pressure (bar)	Stage II desorp- tion pressure (bar)	Stage III desorp- tion pressure (bar)
Three Stage MHHC [32]/2018	3.4 (at 59 °C)	18.4 (at 80 °C)	115.4 (at 100 °C)
Three Stage MHHC [31]/2012	16 (at 100 °C)	36 (at 100 °C)	92 (at 100 °C)
Developed Three Stage MHHC/2025	55 (at 70 °C)	100 (at 90 °C)	160 (at 45 °C)

Table 9. Comparison of hydrogen compression pressures

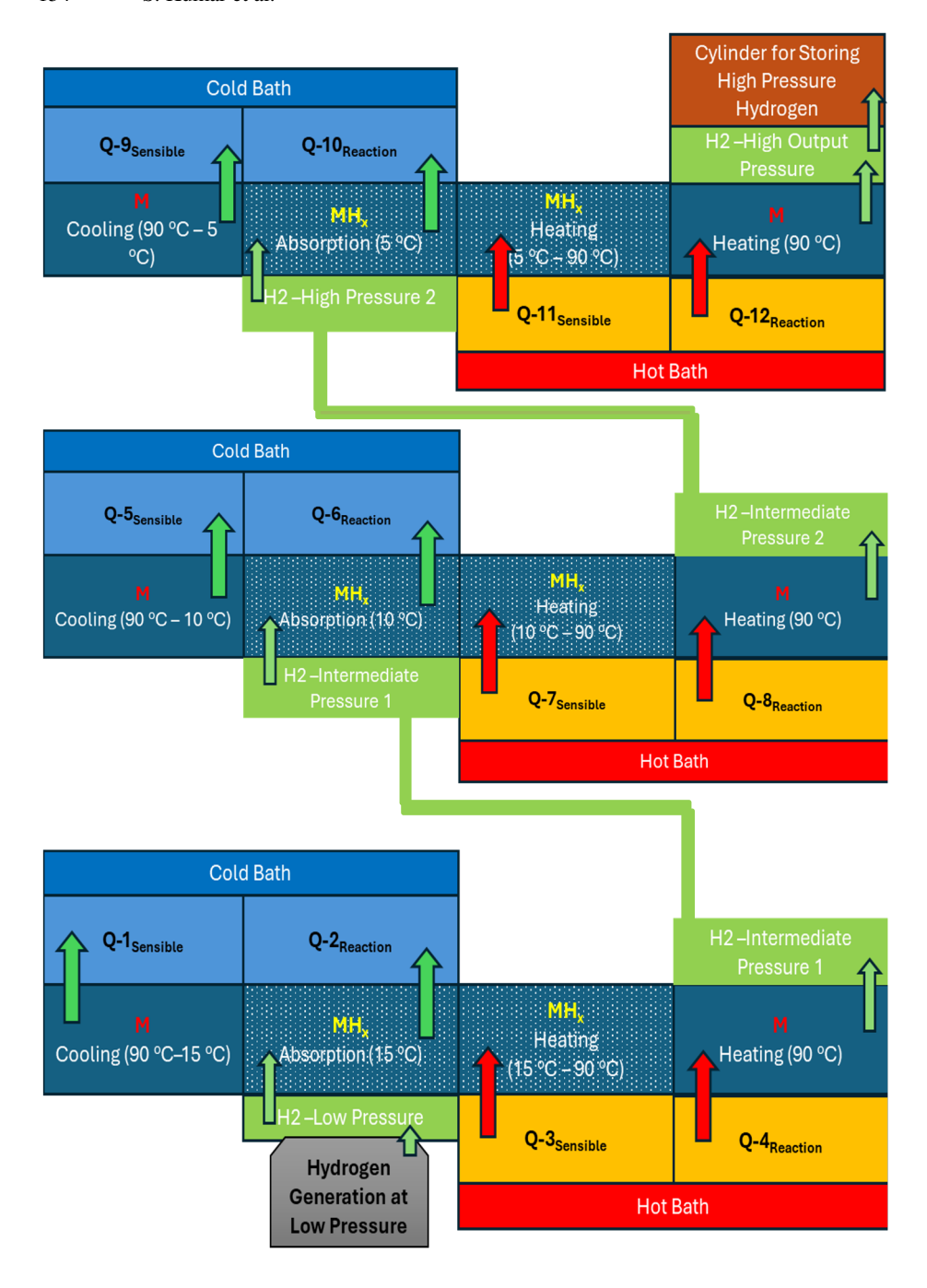


Fig. 17: Heat flow during one complete cycle of three-stage MHHC

# 4 Conclusion

The implementation of a hydrogen microgrid, incorporating solar-driven PEM/SOEC electrolysis and EDR-treated wastewater, demonstrates the technical viability of integrated renewable hydrogen systems for continuous power supply. The development and successful testing of a three-stage metal hydride hydrogen compressor (MHHC), utilizing La<sub>0.8</sub>Ce<sub>0.2</sub>Ni<sub>5</sub>, La<sub>0.5</sub>Ce<sub>0.5</sub>Ni<sub>4</sub>Fe, and Ti<sub>0.8</sub>Zr<sub>0.2</sub>CrMn<sub>0.3</sub>Fe<sub>0.6</sub>Ni<sub>0.1</sub> alloys for successive compression stages, achieved hydrogen output pressures exceeding 150 bar at operating temperatures below 45 °C. The system demonstrated a throughput of 134 L/min, compressing over 200 g of hydrogen in 17 minutes, thereby validating its operational efficiency and reliability under practical conditions.

The MHHC system offers distinct advantages over conventional diaphragm compressors, including lower thermal energy requirements, simplified operation, and reduced maintenance. Future work may focus on optimizing thermal design, increasing the number of stages to achieve higher pressures, and adopting next-generation hydride alloys with improved plateau pressures and absorption/desorption kinetics.

#### Acknowledgements.

M/s Spirare and M/s Ohmium for development and set up of PEM based electrolyser, hydrogen storage and fuel cell system, M/s Green Power International and M/s H2e for development and set up of HTSE system, M/s Central Salt & Marine Chemicals Research for development and set up of EDR system and M/s Fourth Partner Energy Ltd. for development and set up of 4 MWp Solar Unit at NETRA. The development of the 3-stage metal hydride-based hydrogen compressor was a part of collaborative project between IIT Guwahati and NTPC NETRA.

**Disclosure of interests.** The authors have no competing interests to declare that are relevant to the content of this article.

#### References

- 1. Yanez-Barnuevo, M. Microgrids and Energy Improvements in Rural Areas. Environmental and Energy Study Institute (EESI), 2023, Web: https://www.eesi.org/articles/view/microgrids-and-energy-improvements-in-rural-areas, accessed on 27.06.2025
- 2. IRENA. Green hydrogen cost reduction: scaling up Electrolysis to meet the 1.5°C climate goal. In Renew Energy Agency, Abu Dhabi 2020;2020:105.
- 3. Van, L.P., Chi, K. D. & Duc, T. N. Review of hydrogen technologies based microgrid: Energy management systems, challenges and future recommendations. International Journal of Hydrogen Energy 48 (2023) 14127-14148
- Parida, A., Kumar, A., Muthukumar, P., Dalal, A & Kumar, S. Experimental study and performance evaluation of a large-scale multistage metal hydride-based hydrogen compressor. Applied Energy 390 (2025) 125798.
- Sdanghi, G., Maranzana, G., Celzard, A. & Fierro, V. Review of the current technologies and performances of hydrogen compression for stationary and automotive applications. Renewable and sustainable energy reviews, volume 102, March 2019, Pages 15-170.

- 6. Melnik, D., Burger, I., Mitjel, J., Kab, j., Sarkezi-Selsky, P., Jahnke, T. & Knoi, T. Energy efficient cold start of a Polymer Electrolyte Membrane Fuel Cell coupled to a thermochemical metal hydride preheater. Applied Energy 359 (2024) 122585
- 7. Lototskyy, M.V., Yartys, V.A., Pollet, B.G. & Bowman Jr., R.C. Metal hydride hydrogen compressors: review. International Journal of Hydrogen Energy 39 (2014) 5818-5851
- 8. Tarasov, B.P., Bocharnikov, M.S., Yanenko, Y. B., Fursikov, P.V., Minko, K.B. & Lototskyy, M.V. Metal Hydride hydrogen compressors for energy storage systems: layout features and results for long-term tests. J.Phys.: Energy 2(2020)024005
- 9. Yartys, V.A., Lototskyy, M., Linkov, V., Grant, D., Stuart, A., Eriksen, J., Denys, R. & Bowman Jr., R.C. Metal hydride hydrogen compression: recent advances and future prospects. Appl. Phys. A (2016) 122:415
- 10. Chen, Y.H., Shen, C.C., Hsu, C.W. & Lee, S.L. Development of a metal hydride compressor with high-pressure hydrogen storage alloys. Materials Chemistry and Physics 314 (2024) 128917.
- 11. Lototskyy MV, Yartys VA, Pollet BG, Bowman RC. Metal hydride hydrogen compressors: A review. International Journal Hydrogen Energy 2014:39:5818-51.
- 12. Muthukumar P, Kumar A, Raju NN, Malleswararao, K, Rahman MM, A Critical Review on Design Aspects and Developmental Status of Metal Hydride Based Thermal Machines. Int J Hydrogen Energy 2018:43:17753-79.
- 13. Puszkiel, J., von Colbe, J.M.B., Jepsen, J., Mitrokhin, S.V., Movlaev, E., Verbetsky, V. & Klassen, T. Designing an AB2-type Alloy (tiZr-CrMnMo) for the Hybrid Hydrogen Storage Concept. Energies 2020, 13, 2751.
- 14. Karagiorgis, G., Christodoulou, C.N., von Storch, H., Tzamalis, G., Deligiannis, K., Hadjipetrou, D., et al. Design, development, construction and operation of a novel metal hydride compressor. Int J Hydrogen Energy 2017; 42:12364-74.
- 15. NTPC and Indian Army ink PPA for solar-hydrogen microgrid in Ladakh. RenewableWatch, Feb. 2025. Web. https://renewablewatch.in/2025/02/05/ntpc-and-indian-army-ink-ppa-for-solar-hydrogen-microgrid-in-ladakh/ accessed on 29.06.2025.
- 16. Chao, Y.M., & Liang, T.M. A feasibility study of industrial wastewater recovery using electrodialysis reversal. Desalination 221 (2008) 433-439.
- 17. Goodman, N.B., Taylor, R. J., Xie, Z., Gozukara, & Y., Clements, A. A feasibility study of municipal wastewater desalination using electrodialysis reversal to provide recycled water for horticultural irrigation. Desalination 317 (2013) 77-83.
- 18. Sedighi, M., Usefi, M.M.B., Ismail, A.F., & Ghasemi, M. Environmental sustainability and ions removal through electrodialysis desalination: Operating conditions and process parameters. Desalination 549 (2023) 116319.
- 19. Kunrath, C.C.N., Patrocinio, D.C., Rodrigues, M.A.S., Benvenuti, & T., Amado, F.D.R. Electrodialysis reversal as an alternative treatment for producing drinking water from brackish river water: A case study in the dry season, northeastern Brazil. Journal of Environmental Chemical Engineering 8 (2020) 103719.
- 20. R. Bailon, J. Rodriguez & A. Woocay (2021). Energy Efficiency Analysis of a PEM Electrolyzer and a PEM Hydrogen Fuel Cell. Derechos Reservados @2021, SOMIM ISSN 2448-5551.
- 21. Yoon, K.J., Lee, S., Park, S.Y. & Minh, N.Q. Advances in high-temperature solid oxide electrolysis technology for clean hydrogen and chemical production: materials, cells, stacks, systems and economics. Progress in Materials science 154 (2025) 101520.
- 22. Okonkwo, P.C., Ige, O.O., et.el. Platinum degradation mechanisms in proton exchange membrane fuel cell (PEMFC) system: A review. International Journal of Hydrogen Energy 46 (2021) 15850-15865.

- 23. Dong., X., Zhao, H., Li, H., Fucucci, G., Zheng, Q., Zhao, H. et al. A novel design of a metal hydride reactor integrated with phase change material for H2 storage. Appl Energy 2024; 367:123321.
- 24. Wang, D., Wang, Y., Wang, F., Zheng, S., Guan, S., Zheng, L., et al. Optimal design of disc mini-channel metal hydride reactor with high hydrogen storage efficiency. Appl Energy 2022;308.
- 25. Ye, Y., Zhu, H., Cheng, H., Miao, H., Ding, J. & Wang, W. Performance optimization of metal hydride hydrogen storage reactors based on PCM thermal management. Appl Energy 2023: 338:120923.
- 26.ASME. ASME Boiler and Pressure Vessel Code: Section II Part A. 2020.
- 27.ASME. ASME Boiler and Pressure Vessel Code: Section II Part D. 2011.
- 28.Yartys, V.A., Lototskyy, M., Linkov, V., Grant, D., Stuart, A., Eriksen, J., Denys, R. & Bowman Jr., R.C. Metal hydride hydrogen compression: recent advances and future prospects. Appl. Phys. A (2016) 122:415.
- 29. Chesalkin, A., Martaus, A., Averina, J.M. & men'shikov, V.V. La-Ni Based Alloy Modification by Ce and Fe for the next Hydrogen Storages in Low-Temperature Metal Hydrides. ISSN 1067-8212, Russian Journal of Non-Ferrous Metals, 2019, Vol. 60, No. 4, pp. 492-498. @Allerton Press Inc. 2019.
- 30.Li, Q., Peng, Z., Jiang, W., Quyang, L., Wang, H., Liu, J. & Zhu, M. Optimization of Ti-Zr-Cr-Fe alloys for 45 MOA metal hydride hydrogen compressors using orthogonal analysis. Journal of Alloys and Compounds 889 (2021) 161629Li, Q., Peng, Z., Jiang, W., Quyang, L., Wang, H., Liu, J. & Zhu, M. Optimization of Ti-Zr-Cr-Fe alloys for 45 MOA metal hydride hydrogen compressors using orthogonal analysis. Journal of Alloys and Compounds 889 (2021) 161629.
- 31. Muthukumar, P., Patel, K.S., Sachan, P. & Singhal, N. Computational study on metal hydride based three-stage hydrogen compressor. Int J Hydrogen Energy 2012; 37:3797-806.
- 32.Galvis, E.A.R., Leardini, F., Ares, J.R., Cuevas, F. & Fernandez, J.F. Simulation and design of a three-stage metal hydride hydrogen compressor based on experimental thermodynamic data. Int J Hydrogen Energy 2018; 43:6666-76.
- 33.Kelly, N.A. & Girdwood, R. Evaluation of a thermally driven metal-hydride-based hydrogen compressor. Int J Hydrogen Energy 2012; 37:10898-916.

**Open Access** This chapter is licensed under the terms of the Creative Commons Attribution-NonCommercial-NoDerivatives 4.0 International License (http://creativecommons.org/licenses/by-nc-nd/4.0/), which permits any noncommercial use, sharing, distribution and reproduction in any medium or format, as long as you give appropriate credit to the original author(s) and the source, provide a link to the Creative Commons license and indicate if you modified the licensed material. You do not have permission under this license to share adapted material derived from this chapter or parts of it.

The images or other third party material in this chapter are included in the chapter's Creative Commons license, unless indicated otherwise in a credit line to the material. If material is not included in the chapter's Creative Commons license and your intended use is not permitted by statutory regulation or exceeds the permitted use, you will need to obtain permission directly from the copyright holder.

